

Mutually-Aware Feature Learning for Few-Shot Object Counting

Yerim Jeon^a, Subeen Lee^a, Jihwan Kim^a and Jae-Pil Heo^{a,b,*}

^aDepartment of Artificial Intelligence, Sungkyunkwan University, Suwon, 16419, South Korea

^bDepartment of Computer Science and Engineering, Sungkyunkwan University, Suwon, 16419, South Korea

ARTICLE INFO

Keywords:

Few-shot object counting
Class-agnostic counting
Object counting
Few-shot learning
Deep learning

ABSTRACT

Few-shot object counting has garnered significant attention for its practicality as it aims to count target objects in a query image based on given exemplars without the need for additional training. However, there is a shortcoming in the prevailing extract-and-match approach: query and exemplar features lack interaction during feature extraction since they are extracted unaware of each other and later correlated based on similarity. This can lead to insufficient target awareness of the extracted features, resulting in target confusion in precisely identifying the actual target when multiple class objects coexist. To address this limitation, we propose a novel framework, Mutually-Aware FEAture learning (MAFEA), which encodes query and exemplar features mutually aware of each other from the outset. By encouraging interaction between query and exemplar features throughout the entire pipeline, we can obtain target-aware features that are robust to a multi-category scenario. Furthermore, we introduce a background token to effectively associate the target region of query with exemplars and decouple its background region from them. Our extensive experiments demonstrate that our model reaches a new state-of-the-art performance on the two challenging benchmarks, FSCD-LVIS and FSC-147, with a remarkably reduced degree of the target confusion problem.

1. Introduction

Object counting has achieved remarkable advances along with deep learning networks. However, most existing object counting methods are designed for a limited number of categories such as human ? or car ?. In fact, those methods highly rely on a large amount of labeled data and cannot handle unseen categories beyond training data. In this regard, few-shot object counting Lu, Xie and Zisserman (2019) has been proposed to count arbitrary class objects in a query image based on the given exemplar images.

A mainstream of few-shot object counting is the extract-and-match approach Lu et al. (2019); Yang, Su, Hsu and Chen (2021); Ranjan, Sharma, Nguyen and Hoai (2021); Shi, Lu, Feng, Liu and Cao (2022); Gong, Zhang, Yang, Dai and Schiele (2022); You, Yang, Luo, Lu, Cui and Le (2023); Lin, Yang, Ma, Gao, Liu, Liu, Hou, Yi and Chan (2022); Liu, Zhong, Zisserman and Xie (2022); Djukić, Lukežić, Zavrtanik and Kristan (2023); Gao and Huang (2024). Generally, this pipeline consists of three key components: 1) feature extractor, 2) relation learner, and 3) decoder. Firstly, they compute query and exemplar features using the feature extractor, then construct the correlation volume through the relation learner. Afterward, they estimate the number of instances in the query image by transferring the correlation volume to the decoder.

Although previous studies You et al. (2023); Djukić et al. (2023) have achieved impressive performance, they exhibit a target confusion issue, failing to accurately identify only the target class when multiple classes of objects coexist in the query image, as shown in Figure 1. Existing methods

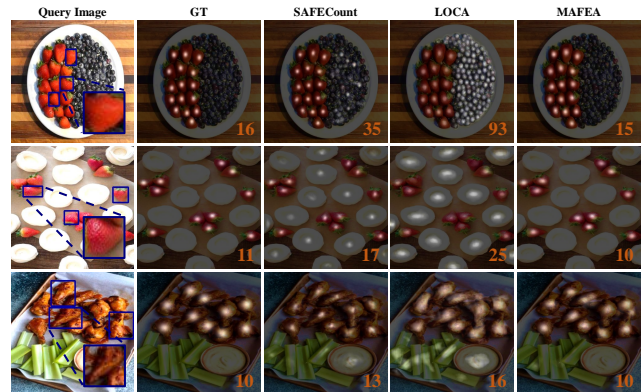


Figure 1: Target confusion problem in a multi-class scenario. Each box in the query image is a box annotation of an exemplar. While SAFECount and LOCA count all objects in the query image regardless of the given exemplar images, MAFEA accurately distinguishes target objects based on the exemplars.

have overlooked this problem, which is directly connected to the purpose of few-shot object counting, as benchmark datasets such as FSC-147 Ranjan et al. (2021) primarily consist of single-class scenes. The main reason for the target confusion is that the query features are computed without any explicit guidance of the target class. Consequently, the query features tend to focus on objectness rather than target class-specific features, hindering the differentiation between target and non-target object features.

To address this, we propose a novel framework, Mutually-Aware FEAture Learning (MAFEA), which enables the early consideration of mutual relations between query and exemplar features to produce the target class-specific features. Specifically, MAFEA employs cross-attention to capture bi-directional co-relations between query and exemplar

*Corresponding author at: Department of Artificial Intelligence, Sungkyunkwan University, Suwon, 16419, South Korea. E-mail addresses: jyr990330@gmail.com (Y. Jeon), leesb7426@gmail.com (S. Lee), damien911224@gmail.com (J. Kim), jaepilheo@skku.edu (J.-P. Heo)

ORCID(s):

features, along with self-attention to reflect internal relationships. With the cross-attention operating in a unified embedding space, the model can identify the difference between the target and non-target object features based on the exemplar features. However, in the cross-attention, query background features including non-target object features are inherently expressed by exemplar features since there are no other features except exemplar features. This might blur the distinction between the target and background features. To prevent this, we introduce a background token, which is incorporated alongside exemplar features in both self- and cross-attentions. This token is trained by our newly proposed Target-Background Discriminative (TBD) loss to effectively represent background features, including non-target object features. Consequently, MAFEA can capture the mutual relations beginning from the feature extractor and recognize the target objects clearly in the multi-category scenario as shown in Figure 1.

To sum up, our contributions are as follows:

- To our knowledge, our approach is the first to tackle the target confusion issue, which involves accurately identifying the target class in a multi-class scenario.
- We propose a novel framework, Mutually-Aware Feature Learning, which considers the mutual relationship between query and exemplar features from the outset.
- We introduce the background token and the Target-Background Discriminative loss to ensure a clear distinction between target and background representation.
- Our method achieves state-of-the-art performance over baselines, and its effectiveness in a multi-class scenario is validated through comprehensive experiments.

2. Related Work

2.1. Class-Specific Object Counting

Class-specific object counting aims to count objects of a specific class, such as people ?, animals Arteta, Lempitsky and Zisserman (2016), and cars ?, in the images. For this purpose, traditional methods Leibe, Seemann and Schiele (2005); Wang and Wang (2011); Stewart, Andriluka and Ng (2016) solve the problem with detection-based approaches. Since most datasets provide only point-level supervision, most detection-based methods generate the pseudo-bounding boxes from point-level ground truth and update them in the training phase. However, they often struggle with scale variation and occlusion. To alleviate this problem, regression-based approaches Yan, Yuan, Zuo, Tan, Wang, Wen and Ding (2019); Zhang, Zhou, Chen, Gao and Ma (2016); Wang, Cai, Han, Zhou and Gong (2022); Wang, Cai, Zhou and Gong (2021) have emerged as popular alternatives in object counting, treating the task as dense regression to predict the object density map. This approach adeptly tackles

overlap problems and achieves good performance. However, both of these approaches cannot handle object classes that are not present in the training phase.

2.2. Few-Shot Object Counting

Few-shot object counting aims to count arbitrary categories in the query image with just a few exemplar images. Pioneering methods Lu et al. (2019); Yang et al. (2021); Ranjan et al. (2021); Gong et al. (2022); Gao and Huang (2024) extract query and exemplar features, and leverage exemplar features as a fixed kernel to produce a correlation volume with query features. BMNet+ Shi et al. (2022) addresses a limitation in kernel-based matching mechanisms, which lack flexible channel interactions, by introducing a dynamic similarity metric capturing key exemplar patterns. SAFECOUNT You et al. (2023) suggests a similarity-aware feature enhancement block that combines the advantages of both features and correlation volume. Recently, SPDCN Lin et al. (2022) and LOCA Djukić et al. (2023) integrate the shape and appearance properties of exemplars to reflect diverse object scales.

These methods have achieved impressive performances, but they do not account for the target confusion issue sufficiently. To alleviate this, we introduce a novel framework, Mutual-Aware Feature Learning, which computes the query and exemplar features dependently on each other throughout the process of feature extraction.

2.3. Vision Transformer

Motivated by the great success in the field of natural language processing, extensive studies have been conducted to employ self-attention for vision tasks such as image classification Ramachandran, Parmar, Vaswani, Bello, Levskaya and Shlens (2019); Dosovitskiy, Beyer, Kolesnikov, Weissenborn, Zhai, Unterthiner, Dehghani, Minderer, Heigold, Gelly, Uszkoreit and Houlsby (2021), object detection Carion, Massa, Synnaeve, Usunier, Kirillov and Zagoruyko (2020); Meng, Chen, Fan, Zeng, Li, Yuan, Sun and Wang (2021), and semantic segmentation Yin, Wang, Wang, Xu, Zhang, Li and Jin (2022); Caron, Touvron, Misra, Jégou, Mairal, Bojanowski and Joulin (2021). Also, the transformer-based encoder has advantages in class-specific object counting Tran, Huy, Duong, Nguyen, Hung, Nguyen, Bui, Truong and VinBrain (2022); Liang, Chen, Xu, Zhou and Bai (2022). Recently, for few-shot object counting, CounTR Liu et al. (2022) utilizes a transformer-based architecture to capture self-similarity prior explicitly and shows a powerful performance.

Unlike CounTR, which exploits separate feature extractors for query and exemplar images, MAFEA utilizes a mutually-aware feature extractor, computing the query and exemplar features in a unified embedding space. Moreover, MAFEA clearly distinguishes target object features from background features by introducing the background token.

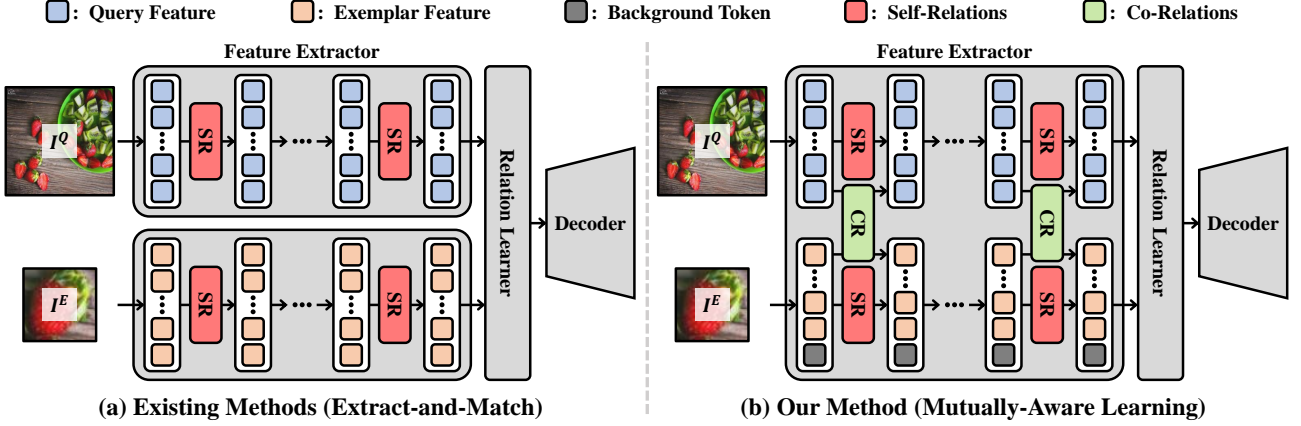


Figure 2: Comparison between Extract-and-Match methods and our proposed MAFEA. (a) Existing methods extract query and exemplar features without any explicit feedback to each other. (b) On the other hand, MAFEA produces the query and exemplar features based on their mutual relation from an early stage of the feature extractor. By integrating self-relations and bi-directional co-relations, MAFEA produces highly target-aware features. Moreover, the learnable background token is fed into the self- and co-relations with the exemplar features to represent the background regions of the query image.

3. Method

In this work, we introduce Mutually-Aware Feature learning (MAFEA) to compute query and exemplar features mutually-aware of each other throughout the feature extractor, while the previous methods compute these features without any explicit feedback to each other, as illustrated in Figure 2. Specifically, MAFEA considers the co-relations between query and exemplar images in addition to the self-relations of each image. Moreover, we introduce a learnable background token to prevent undesired interactions between the exemplar and background features in co-relations. As a result, MAFEA can produce highly target-aware features that differentiate target object features from the background features, including the non-target object features.

3.1. Overall Pipeline

The architecture of MAFEA consists of a ViT encoder, relation learner, and CNN decoder. Firstly, given a query image $I^Q \in \mathbb{R}^{3 \times H^Q \times W^Q}$ and a set of M exemplar images $I^E = \{I_i^E \in \mathbb{R}^{3 \times H_i^E \times W_i^E} | i \in \{1, 2, \dots, M\}\}$ as input, they are split into N^Q and N_i^E image patches of resolution $S \times S$ respectively, where $N^Q = H^Q W^Q / S^2$ for the query image and $N_i^E = H_i^E W_i^E / S^2$ for the exemplar images. Then, image patches are converted into the query features $z^Q \in \mathbb{R}^{N^Q \times C}$ and exemplar features $z_i^E \in \mathbb{R}^{N_i^E \times C}$ by a projection function $\mathbb{R}^{3 \times S \times S} \rightarrow \mathbb{R}^C$. Also, position embedding is added to z^Q and z_i^E to retain positional information, and z_i^E are concatenated to define $z^E \in \mathbb{R}^{N^E \times C}$ where N^E denotes the sum of N_i^E . After that, z^Q and z^E are refined by the ViT encoder, which incorporates mutual relation modeling. Finally, the relation learner and CNN decoder sequentially receive the refined query and exemplar features and produce a density map $y \in \mathbb{R}^{1 \times H^Q \times W^Q}$. The number of objects in the query image is computed as the sum of density map.

3.2. Mutual Relation Modeling

The core idea of MAFEA is to consider the mutual relationship between query and exemplar features from the outset. MAFEA encodes features based on two types of relationships: self-relations within each image, and co-relations between different images. The refined query s^Q and exemplar features s^E , reflecting self-relations, are defined as follows:

$$\begin{aligned} s^Q &= \text{MHA}(Q^Q, K^Q, V^Q), \\ s^E &= \text{MHA}(Q^E, K^E, V^E), \end{aligned} \quad (1)$$

where Q , K , and V represent queries, keys, and values fed to the multi-head attention block (MHA). We compute Q^Q , K^Q , and V^Q by applying linear projections to the given query features z^Q respectively, and produce Q^E , K^E , and V^E using exemplar features z^E . The self-relation modeling guides the query and exemplar features to capture self-similarity within each image. Unlike the previous works only define self-relations throughout the feature extractor, we also refine query $c^{E \rightarrow Q}$ and exemplar features $c^{Q \rightarrow E}$ using co-relations as follows:

$$\begin{aligned} c^{E \rightarrow Q} &= \text{MHA}(Q^Q, K^E, V^E), \\ c^{Q \rightarrow E} &= \text{MHA}(Q^E, K^Q, V^Q). \end{aligned} \quad (2)$$

The correlation modeling enables bi-directional interaction between query and exemplar features. Firstly, the exemplars influence the query by identifying the difference between the target and non-target object features. Secondly, the query contributes to refining the exemplars, enabling them to aggregate diverse target object features. As a result, the encoder refines the query features to focus more on target-specific traits rather than general object characteristics. With self-relations and co-relations, the output sequences of the l -th encoder layer are derived as follows:

$$\begin{aligned} z_{l+1}^Q &= z_l^Q + s_l^Q + c_l^{E \rightarrow Q}, \quad l = 1, 2, \dots, L-1, \\ z_{l+1}^E &= z_l^E + s_l^E + c_l^{Q \rightarrow E}, \quad l = 1, 2, \dots, L-1, \end{aligned} \quad (3)$$

where z_l^Q and z_l^E are the input sequences of the l -th encoder layer. This modeling enables the encoder to adapt features not only based on their inherent self-relations but also their interrelated correlations.

3.3. Background Token

When computing $c^{E \rightarrow Q}$ in Eq. 2, MAFEA utilizes only exemplar features to produce keys and values. Although the attention mechanism intrinsically mitigates improper co-relations, the background features, including non-target object features, might be represented by the exemplar features. In this case, it obscures the difference between the target object and background features, thus, it confuses in precisely identifying the actual target in the query features. In this regard, we introduce the background token which is designed to learn the general features of the background region. The background token $z^B \in \mathbb{R}^{1 \times C}$ is concatenated with the exemplar features and then fed into the self-relation and co-relation modeling as follows:

$$\begin{aligned} s^{[E;B]} &= \text{MHA}([Q^E; Q^B], [K^E; K^B], [V^E; V^B]), \\ c^{[E;B] \rightarrow Q} &= \text{MHA}(Q^Q, [K^E; K^B], [V^E; V^B]), \\ c^{Q \rightarrow [E;B]} &= \text{MHA}([Q^E; Q^B], K^Q, V^Q), \end{aligned} \quad (4)$$

where Q^B , K^B , and V^B are obtained by linear projections on the background token, respectively. $s^{[E;B]}$, $c^{[E;B] \rightarrow Q}$, and $c^{Q \rightarrow [E;B]}$ substitute s^E , $c^{E \rightarrow Q}$, and $c^{Q \rightarrow E}$ defined in Eq. 1 and Eq. 2, individually. By incorporating the background token into those relations, we can prevent the background features from being expressed by the exemplar features in the computation of $c^{[E;B] \rightarrow Q}$.

3.4. Target-Background Discriminative Loss

Although the background token is designed to handle the background features of the query, it is not guaranteed without an explicit objective. In this regard, we define a target-background discriminative (TBD) loss which encourages the background token to align with background features. We first compute alignment score AS_i , which represents the degree of alignment between i -th query feature and the background token, as follows:

$$AS_i = \frac{\sum_{j=1}^{N^B} \left(\exp \left(Q_i^Q \cdot K_j^B \right) \right)}{\sum_{j=1}^{N^E+N^B} \left(\exp \left(Q_i^Q \cdot [K^E; K^B]_j \right) \right)}, \quad (5)$$

where Q_i^Q is i -th Q^Q , and K_j^B and $[K^E; K^B]_j$ denote j -th K^B and $[K^E; K^B]$, respectively. Then, to align the background token only with background features, we divide the query features into positive set P , comprising features that spatially contain one or more ground-truth (GT) points, and negative set N which consists of features not including any GT points. As a result, we define TBD for the i -th query feature, as follows:

$$\mathcal{L}_i^{\text{TBD}} = -\mathbb{1}_{z_i^Q \in P} \log (1 - AS_i) - \mathbb{1}_{z_i^Q \in N} \log (AS_i), \quad (6)$$

where $z_i^Q \in P$ and $z_i^Q \in N$ mean i -th query features belong to the positive set and or not, respectively. Also, \mathcal{L}^{TBD} is the average value of $\mathcal{L}_i^{\text{TBD}}$ over all query features.

3.5. Training Loss

Once obtaining the target-aware features, z^Q and z^E , we produce the correlation volume using the relation learner and convert it to the density map with the decoder. Following Djukić et al. (2023), the relation learner performs iterative adaptation to produce intermediate correlation volumes, subsequently processed by auxiliary decoder blocks as follows:

$$\begin{aligned} C &= \text{Relation-Learner}(z^Q, z^E), \\ y_k &= \text{Decoder}_k(c_k), \quad k = 1, 2, \dots, K, \end{aligned} \quad (7)$$

where $C = \{c_k\}_{k=1}^K$ is the set of correlation volumes and y_k is the output of the k -th decoder.

We adopt the object-normalized l_2 loss ($\mathcal{L}^{\text{count}}$), which is the mean squared error between the predicted and ground truth density map normalized by the number of objects. The object-normalized l_2 loss is formulated as follows:

$$\mathcal{L}^{\text{count}} = \frac{1}{M} \|\|y - \hat{y}\|_2^2, \quad (8)$$

where y and \hat{y} are the predicted density and ground-truth density maps, respectively. M is the number of objects in mini-batch. Also, we utilize the auxiliary loss (\mathcal{L}^{aux}) for the intermediate density maps as follows:

$$\mathcal{L}^{\text{aux}} = \frac{1}{M} \sum_{k=1}^{K-1} \|\|y_k - \hat{y}\|_2^2, \quad (9)$$

where y_k is the intermediate density map of the k -th decoder and $K - 1$ is the number of intermediate density maps. The full objectives are defined as follows:

$$\mathcal{L} = \mathcal{L}^{\text{count}} + \lambda_1 \mathcal{L}^{\text{aux}} + \lambda_2 \mathcal{L}^{\text{TBD}}, \quad (10)$$

where λ_1 and λ_2 are the weights of the auxiliary loss and TBD loss, respectively.

4. Experiments

In this section, we first describe the experimental settings. We then compare it with the current state-of-the-art methods. Finally, we provide in-depth analyses of the results through the various ablation studies.

4.1. Implementation Details

4.1.1. Architecture.

Our framework comprises a ViT encoder, relation learner, and CNN decoder. The patch size is set to 16×16 , and both the kernel and stride of the projection head are set to 16×16 corresponding to the patch size. The ViT encoder comprises 12 transformer encoder blocks where the hidden dimension of each block is 768, and the multi-head attention of each block consists of 12 heads. The relation learner, inspired by

Table 1

Image indices of FSC-147-Multi. The subset consists of 31 and 12 images in the validation and test set, respectively.

Eval Set	Indices
Val	216, 236, 243, 244, 252, 752, 913, 1930, 1999, 2303, 2305, 2306, 2826, 2830, 2837, 2868, 2872, 2875, 2890, 3520, 3592, 3785, 3979, 3980, 4102, 4851, 5103, 5105, 5111, 5669, 6872
Test	336, 343, 344, 681, 2143, 3114, 4495, 4885, 4920, 4921, 5379, 6732

LOCA Djukić et al. (2023), incorporates Object Prototype Extraction (OPE) modules and Prototype Matching (PM). OPE integrates object shapes and appearance properties using a three-layered iterative adaption module. Each layer includes two multi-head attention blocks and a feed-forward network. Instead of ROI pooled features, we utilize exemplar features as appearance properties. PM involves the depth-wise correlation and max operation. Further details are provided in the appendix. The CNN decoder comprises 4 convolutions and bilinear upsampling layers to regress a 2D density map. The ViT encoder is initialized with a self-supervised pre-trained weight from MAEHe, Chen, Xie, Li, Dollár and Girshick (2022). On the other hand, the parameters of the relation learner and CNN decoder are randomly initialized.

4.1.2. Training details.

We apply the same pre-processing as LOCA. As the inputs, the query image is resized to 512×512 and exemplar images are scaled to 48×48 based on provided box annotations. We set the weights λ_1 and λ_2 for auxiliary and TBD loss in Eq. 10 to 0.3 and 0.05, respectively. AdamW optimizer is employed with a batch size of 8. The initial learning rate is $1e^{-4}$ and is halved every 40 epochs. Training is performed on a single RTX3090 GPU for 100 epochs.

4.2. Datasets and Metrics.

4.2.1. Datasets.

We experiment on three benchmark datasets: FSCD-LVIS Nguyen, Pham, Nguyen and Hoai (2022), FSC-147 Ranjan et al. (2021), and CARPK Hsieh, Lin and Hsu (2017). FSCD-LVIS is designed for few-shot object counting and detection in complex scenes with multiple class objects. It contains 6195 images across 372 classes, split into 3953 train and 2242 test images. FSC-147, a few-shot object counting dataset, consists of simpler scenes where most images contain only a target class. It includes 6135 images of 147 classes, divided into 3659 train, 1286 validation, and 1190 test images. Both datasets include three randomly selected exemplars per image to depict the target objects. Note that, there is no shared object class between the sets. Furthermore, we validate our models' generalization capability on the test set of CARPK, a dataset tailored for counting cars, comprising 459 drone-captured images.

4.2.2. Configuration of Multi-Class Subset.

Although the FSC-147 contains a large number of objects in each image, the scene of each image is mostly composed of single-class objects. Due to this inherent characteristic, the evaluation of the FSC-147 might not accurately assess the ability of the model to identify the target class within an image containing diverse object categories. For a quantitative assessment of whether the model suffers from the target confusion problem, we construct a multi-class subset of the FSC-147 (FSC-147-Multi). We selectively remove images where objects from other classes amount to less than 20% of the target class objects, to exclude single-object predominant images in the multi-class experiments. The indices of the images that make up the FSC-147-Multi can be found in Table 1, and experimental results are detailed in Sec. 4.3.

4.2.3. Metrics.

Generally, the counting methods are evaluated using Mean Absolute Error (MAE) and Root Mean Squared Error (RMSE). These metrics are defined as follows:

$$\text{MAE} = \frac{1}{n} \sum_{i=1}^n |y_i - \hat{y}_i|, \quad (11)$$

$$\text{RMSE} = \sqrt{\frac{1}{n} \sum_{i=1}^n (y_i - \hat{y}_i)^2},$$

where n denotes the number of images, y_i and \hat{y}_i are the ground truth and predicted counts for i -th image, respectively.

4.3. Comparison with the State-of-the-Art

To evaluate the model's robustness against target confusion, assessments need to be conducted in multi-class scenes where diverse class objects coexist. Given that the FSC-147 dataset mainly consists of simple scenes with only target class objects, its limited multi-class scenes are not suitable for target confusion evaluation. Thus, we construct a multi-class subset of the FSC-147 (FSC-147-Multi), where images contain non-target objects more than 20 % of the number of existing target class objects. Initially, we compare our model with state-of-the-art (SOTA) methods in a complex multi-class scenario, and then extend the evaluation to a simpler single-class scenario.

4.3.1. Evaluation on a multi-class scenario

We compare our method with SOTA methods on multi-class datasets: FSCD-LVIS and FSC-147-Multi, as shown in Table 2. For a fair comparison on FSCD-LVIS, we reproduce all baseline models using an image size of 512 by utilizing official codes. Regarding Counting-DETR, we report its official performance. On the FSCD-LVIS, our method outperforms all baselines, showing an improvement of 11 % in MAE and 4.6 % in RMSE compared to the second-best performer. Similarly, on the FSC-147-Multi, our results demonstrate a significant performance gap compared to the

Table 2

Evaluation on a multi-class scenario with 3-shot exemplars. The results on FSCD-LVIS are reproduced using the official implementation, employing identical query image sizes of 512. The results on the multi-class subset of FSC-147 (FSC-147-Multi) are evaluated using the official pre-trained weights. The subset consists of 31 (over 1286) in the validation set and 12 (over 1190) images in the test set, totaling 43 images. ‘-’ means that the score is not available. ‘†’ means the mean and standard deviation of the results over five runs with 95% confidence intervals.

Method	FSCD-LVIS		FSC-147-Multi	
	MAE ↓	RMSE ↓	MAE ↓	RMSE ↓
Counting-DETR Nguyen et al. (2022)	23.50	35.89	-	-
BMNet+ Shi et al. (2022)	17.04	27.71	11.22	16.99
SPDCN Lin et al. (2022)	14.36	26.31	9.27	13.54
CounTR Liu et al. (2022)	14.14	26.01	16.12	30.70
SAFECount You et al. (2023)	14.01	24.04	8.63	12.18
LOCA Djukić et al. (2023)	14.38	24.28	9.97	16.83
MAFEA (Ours)	12.47	22.94	6.36	9.18
LOCA [†] Djukić et al. (2023)	14.51 ± 0.12	24.70 ± 0.88	10.41 ± 0.69	17.29 ± 1.63
MAFEA [†] (Ours)	12.51 ± 0.09	23.11 ± 0.09	5.52 ± 0.66	7.93 ± 1.06

Table 3

Evaluation on a single-class scenario with 3-shot exemplars in FSC-147 dataset. ‘†’ indicates the mean and standard deviation of the results over five runs with 95% confidence intervals.

Method	Val		Test	
	MAE ↓	RMSE ↓	MAE ↓	RMSE ↓
GMN Lu et al. (2019)	29.66	89.81	26.52	124.57
FamNet Ranjan et al. (2021)	24.32	70.94	22.56	101.41
CFOCNet Yang et al. (2021)	21.19	61.41	22.10	112.71
RCAC Gong et al. (2022)	20.54	60.78	20.21	81.86
Counting-DETR Nguyen et al. (2022)	-	-	16.79	123.56
BMNet+ Shi et al. (2022)	15.74	58.53	14.62	91.83
SPDCN Lin et al. (2022)	14.59	49.97	13.51	96.80
CounTR Liu et al. (2022)	13.13	49.83	11.95	91.23
SAFECount You et al. (2023)	15.28	47.20	14.32	85.54
LOCA Djukić et al. (2023)	10.24	32.56	10.79	56.97
CSTrans Gao and Huang (2024)	18.10	58.45	16.38	93.51
MAFEA (Ours)	8.92	32.45	9.84	56.68
LOCA [†] Djukić et al. (2023)	10.57 ± 0.19	34.30 ± 1.79	11.39 ± 0.32	72.82 ± 7.16
MAFEA [†] (Ours)	9.24 ± 0.22	33.88 ± 0.74	10.23 ± 0.40	64.96 ± 5.65

SOTA method, showing a relative improvement of 26.30 % in MAE and 24.63 % in RMSE.

4.3.2. Evaluation on a single-class scenario

We further evaluate our method on the validation and test sets of the FSC-147 dataset, as shown in Table 3. Our method surpasses all baselines, showing an enhancement in MAEs of 12.9% and 8.8% for validation and test sets, respectively. It demonstrates the effectiveness of MAFEA even in a single-class scenario. In addition, we report the mean and standard deviation of results with 95% confidence intervals over five runs. Notably, the test set’s RMSE exhibits a high standard deviation. To analyze a factor influencing test RMSE, we conduct evaluations by excluding extremely high-dense images with over 1000 instances. A total of 2 (over 1190) images are excluded from the test set. This exclusion leads to a notable improvement in LOCA’s RMSE, decreasing from 56.97 to 32.85 (42.3%). Similarly, MAFEA’s performance dramatically improves with RMSE decreasing from 56.68

to 34.35 (39.4%). This confirms the sensitivity of RMSE to errors in high-dense images and indicates the dependency of RMSE on how well the model fits extremely high-dense images.

4.3.3. Qualitative results

In Fig. 3, the 1st and 2nd rows illustrate qualitative results of the FSCD-LVIS. As shown in the 3rd to 6th columns, prior methods struggle to identify the target class in a query using exemplar images; they often count not only target objects but also non-target objects sharing similar scale or appearance properties. In contrast, our method excels in precisely distinguishing target objects based on the exemplar images, a success attributable to our mutually-aware feature learning. The 3rd and 4th rows show the results for the FSC-147. Our method makes more accurate predictions compared to other methods, especially on dense images.

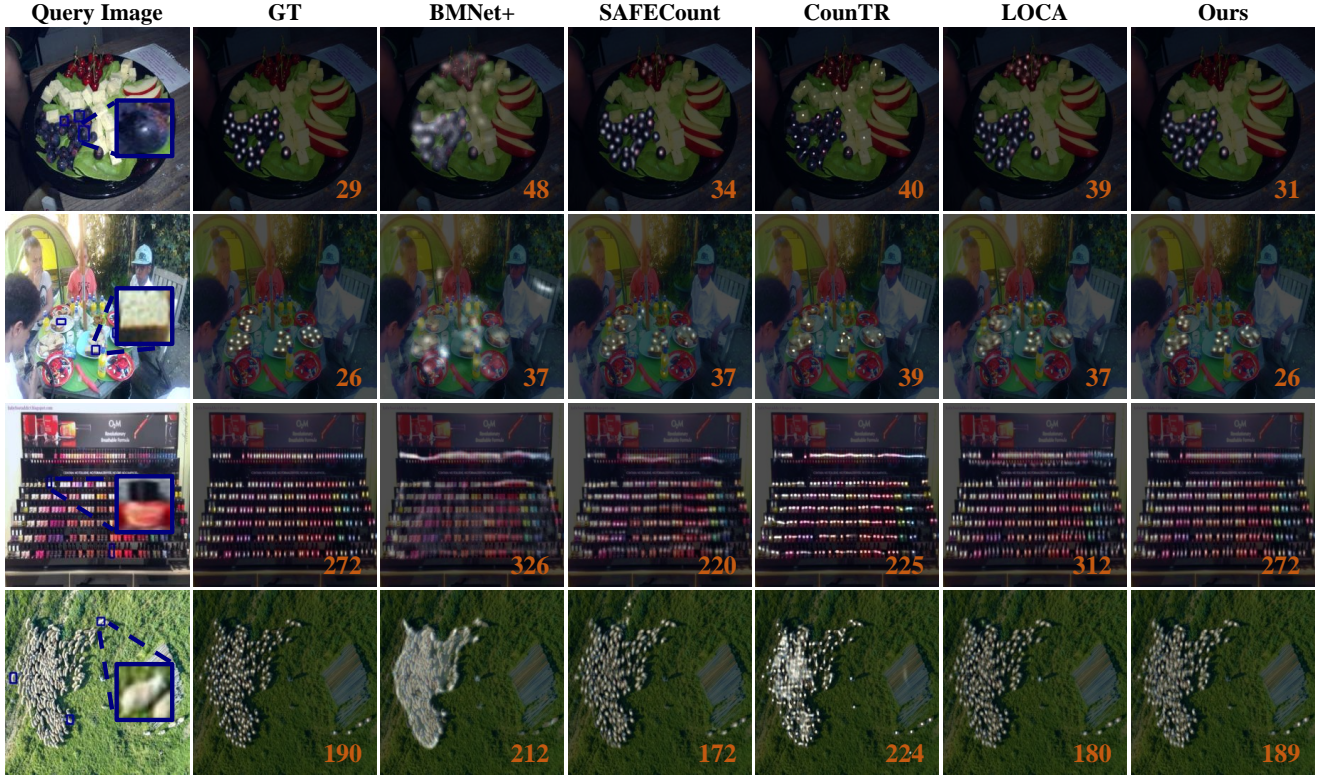


Figure 3: Qualitative results: 1st and 2nd rows from FSCD-LVIS dataset, and the 3rd and 4th rows from FSC-147 dataset. Each box in the query image is a box annotation for an exemplar, while the numbers in the pictures are the counting results. Best viewed with zoom-in.

Table 4
Cross-dataset generalization performance on CARPK.

Method	CARPK	
	MAE ↓	RMSE ↓
GMN Lu et al. (2019)	32.92	39.88
FamNet Ranjan et al. (2021)	28.84	44.47
RCAC Gong et al. (2022)	17.98	24.21
BMNet+ Shi et al. (2022)	10.44	13.77
SPDCN Lin et al. (2022)	18.15	21.61
SAFECount You et al. (2023)	16.66	24.08
LOCA Djukić et al. (2023)	9.97	12.51
CSTrans Gao and Huang (2024)	20.84	24.64
MAFEA (ours)	9.19	11.90

4.4. Cross-Dataset Generalization

We evaluate the generalization ability of our model on a car counting dataset, CARPK. To avoid overlap between the train and test sets, the tested models are pre-trained with FSC-147 by excluding its car category. The results are summarized in Table 4. Note that, we do not fine-tune our model on the CARPK. As reported, our method outperforms the current state-of-the-art methods. It demonstrates the robustness of our method in cross-dataset generalization.

4.5. Ablation Study

To verify the effectiveness of our approach, we conduct extensive ablation studies on FSCD-LVIS and FSC-147.

Table 5

Ablation study on Mutual Relation Modeling (MRM), Background Token (BT), and Target-Background Discriminative (TBD) Loss in FSCD-LVIS. 'ALL' denotes the performance on the entire area of the image. 'Target' denotes performance within the area encompassing all target objects, and 'Non-Target' signifies performance in the complementary area.

MRM	BT	TBD	ALL		Target		Non-Target	
			MAE	RMSE	MAE	RMSE	MAE	RMSE
.	.	.	14.89	25.95	18.64	28.84	15.65	23.52
✓	.	.	13.90	25.04	13.88	24.33	10.12	18.22
✓	✓	.	13.28	24.13	13.69	24.26	9.91	16.42
✓	✓	✓	12.47	22.94	12.70	22.62	7.54	14.88

Specifically, we begin with component-level analysis on multi-class and single-class scenarios and then investigate the impact of the number of exemplars. Additionally, we visualize the attention maps of the Alignment Score (AS) map to validate the role of the background token.

4.5.1. Component-level analysis on multi-class scenario

Firstly, we verify the effect of integrating mutual relation modeling into the feature extractor. In Table 5 and Table 6, the 1st row presents the result of the model that independently computes query and exemplar features by a shared feature extractor. Compared with it, MRM shows noteworthy

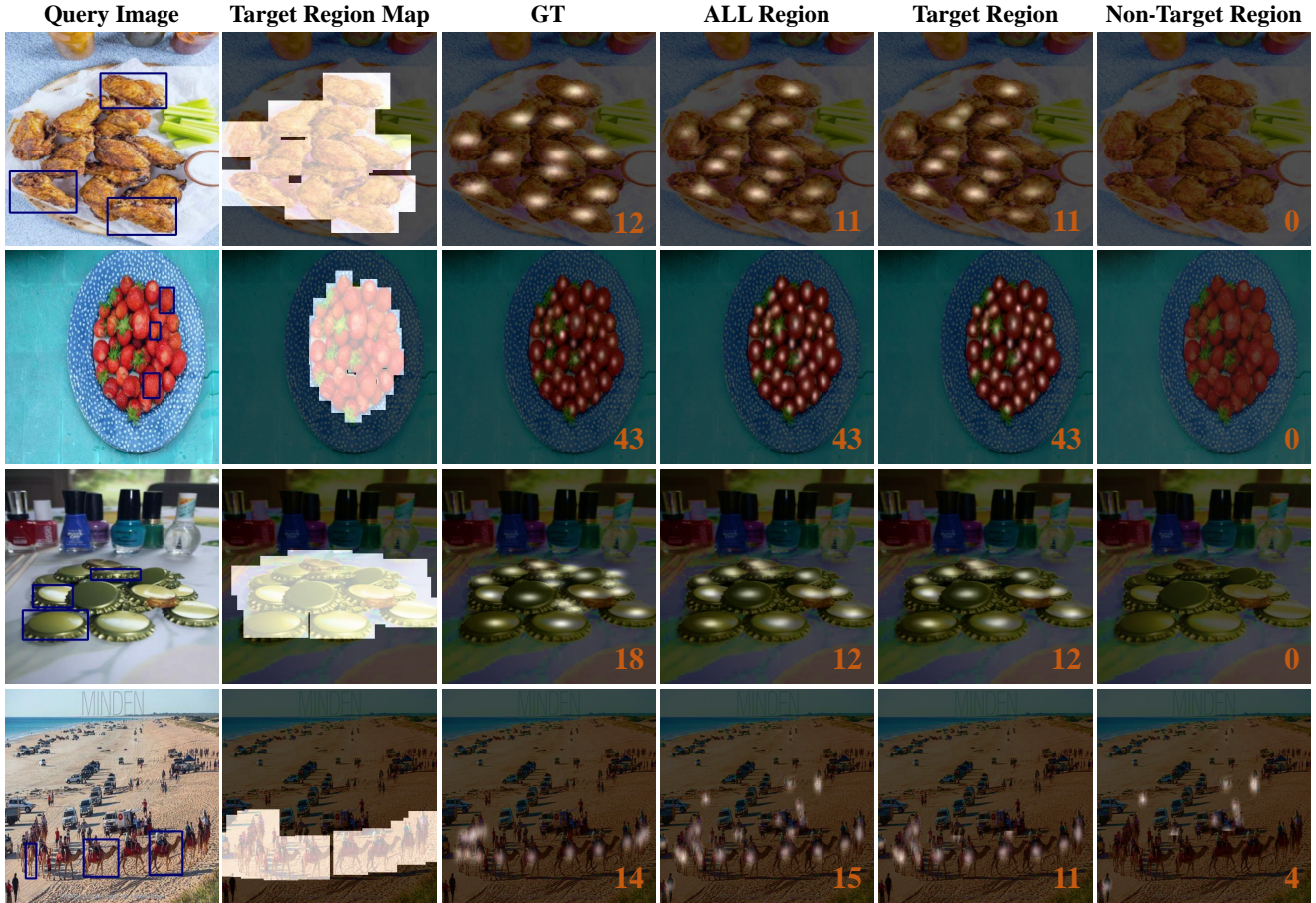


Figure 4: Results in multi-class scenes within the FSC-147 dataset. From left to right: query image, target region map, ground-truth density map, our prediction on all region, target region, and non-target region. Each box in the query image is a box annotation for each exemplar image, while the numbers in images are the counting results.

Table 6

Ablation study on Mutual Relation Modeling (MRM), Background Token (BT), and Target-Background Discriminative (TBD) Loss in FSC-147-Multi. ‘ALL’ denotes the performance on the entire area of the image. ‘Target’ denotes performance within the area encompassing all target objects, and ‘Non-Target’ signifies performance in the complementary area.

MRM	BT	TBD	ALL		Target		Non-Target	
			MAE	RMSE	MAE	RMSE	MAE	RMSE
.	.	.	12.01	21.81	7.84	15.13	5.85	11.13
✓	.	.	8.26	11.90	5.65	9.29	3.34	6.44
✓	✓	.	7.40	11.39	5.42	8.07	2.80	5.97
✓	✓	✓	6.36	9.18	4.58	6.84	2.60	5.20

enhancements in both datasets, with a 6.6% MAE gain in FSCD-LVIS, and a 31.2% MAE improvement in FSC-147-Multi. This highlights the importance of mutual awareness in computing query and exemplar features. Subsequently, we delve into the impact of BT and TBD loss. As shown in the 3rd and 4th rows, while BT yields a slight performance improvement when used alone, its combination with TBD

loss leads to a notable performance enhancement. BT brings a performance gain of 4.5% MAE in FSCD-LVIS and 10.4% MAE in FSC-147-Multi, while the TBD loss achieves an additional performance gain of 6.1% MAE in FSCD-LVIS and 14.1% in FSC-147-Multi. It demonstrates that minimizing undesired interactions between query and exemplar features enhances target recognition of the model.

Furthermore, we assess performance in the target and non-target regions to verify whether the models count only the target objects. This is imperative since the evaluation within the entire region may compensate for potential under-predictions in the target region by incorrect predictions in the non-target region. In the few-shot object counting (FSOC), each object is annotated only with its center point, which is not sufficient to estimate good boundaries between the target region and non-target region. To overcome this limitation, we expand each point annotation to encompass an area equivalent to the maximum size of exemplars. Consequently, the target region encompasses all target objects, while the non-target region covers the complementary area. We provide the visualization of the target region map and corresponding results in Figure 4. If there is no target confusion issue, the model’s prediction in the non-target region

Table 7

Ablation study on Mutual Relation Modeling (MRM), Background Token (BT), and Target-Background Discriminative Loss (TBD) in the FSC-147 dataset.

MRM	BT	TBD	Val		Test	
			MAE ↓	RMSE ↓	MAE ↓	RMSE ↓
.	.	.	12.43	42.97	12.91	77.89
✓	.	.	10.94	34.56	11.43	71.43
✓	✓	.	10.04	36.47	10.78	88.43
✓	✓	✓	8.92	32.45	9.84	56.68

Table 8

Impact of the number of exemplars

Shot	FSCD-LVIS		FSC-147					
	Test		Multi		Val		Test	
	MAE	RMSE	MAE	RMSE	MAE	RMSE	MAE	RMSE
0	14.72	27.42	12.12	26.51	14.54	60.44	13.23	105.99
1	13.30	24.26	8.32	18.80	11.14	42.37	11.68	99.17
2	12.81	23.68	6.52	15.32	10.79	42.04	10.91	80.74
3	12.47	22.94	6.36	9.18	8.92	32.45	9.84	56.68

should be zero. Impressively, MRM, BT, and TBD bring substantial performance improvements in both target and non-target areas. The notable enhancement in the non-target area validates that the proposed components alleviate target confusion as intended.

4.5.2. Component-level analysis on single-class scenario

We further assess our proposed module in the validation and test sets of FSC-147. As shown in Table 7, MRM achieves a performance gain of 12.0% MAE and 11.5% MAE for the validation and test sets, respectively. The ablation of BT brings an improvement of 8.2% MAE and 5.7% MAE for the validation and test sets, respectively. Also, TBD brings an improvement in MAEs of 11.2% and 8.7% for validation and test sets, respectively. These results confirm the effectiveness of our method even in the single-class scenario.

4.5.3. The number of exemplars

We further investigate the impact of the exemplar's numbers in Table 8. From the zero-shot where exemplar features are replaced by learnable tokens, to the 3-shot, our method provides better performance as more exemplars are provided. These results validate that the exemplar features contribute to refining the query features in a mutually-aware manner.

4.5.4. Influence of the background token

To validate whether the background token highlights the background region, we visualize the alignment score (AS) map in Fig. 5. We also compute the AS map for the exemplar features by summing up the scores of these features. As shown in the Fig. 5, the exemplar features activate only the

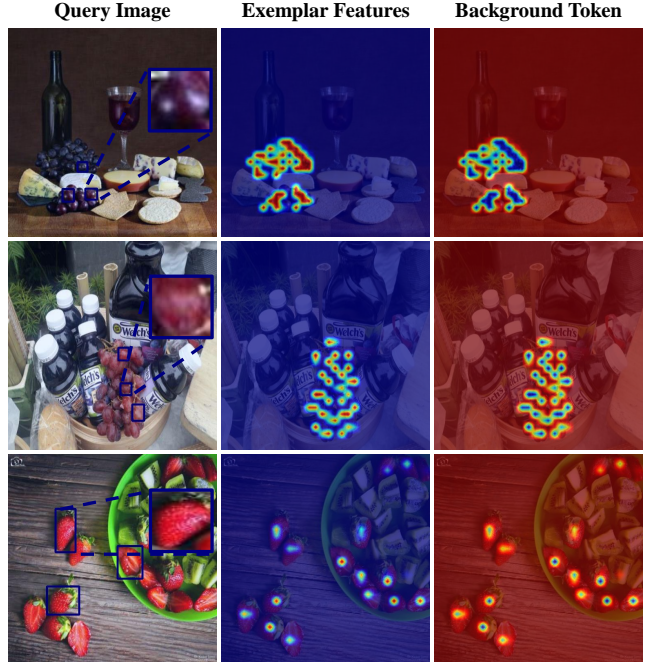


Figure 5: Alignment Score (AS) map of exemplar features and background token.

target areas, while the background token highlights the background areas including the non-target class objects. These results show that our model can effectively differentiate between target objects and background regions.

4.6. Additional Qualitative Results

We show more qualitative results. As reported in Figure 6a, we can observe that our model makes precise predictions from sparse to dense scenes for the novel classes. However, as seen in Figure 6b, accurate predictions are challenging for images with over 1000 instances, which are very dense. This issue is not unique to MAFEA. Given the practical application of few-shot object counting models, we believe that having 1000 objects within a single image is an uncommon scenario.

5. Conclusion

In this work, we discover and solve the target confusion problem, which arises when multiple object classes coexist in the query image, resulting in inaccurate identification of the target objects. To settle this problem, we introduce a novel perspective, Mutually-Aware Feature Learning (MAFEA), which encourages interaction between query and exemplar features from the outset. By incorporating mutual relation modeling into the feature extractor, our model produces highly target-aware query features, facilitating the distinction between target and non-target objects. Additionally, the background token with Target-Background Discriminative (TBD) loss enables the model to effectively differentiate target objects from background features. We demonstrate the robustness of our method against the target

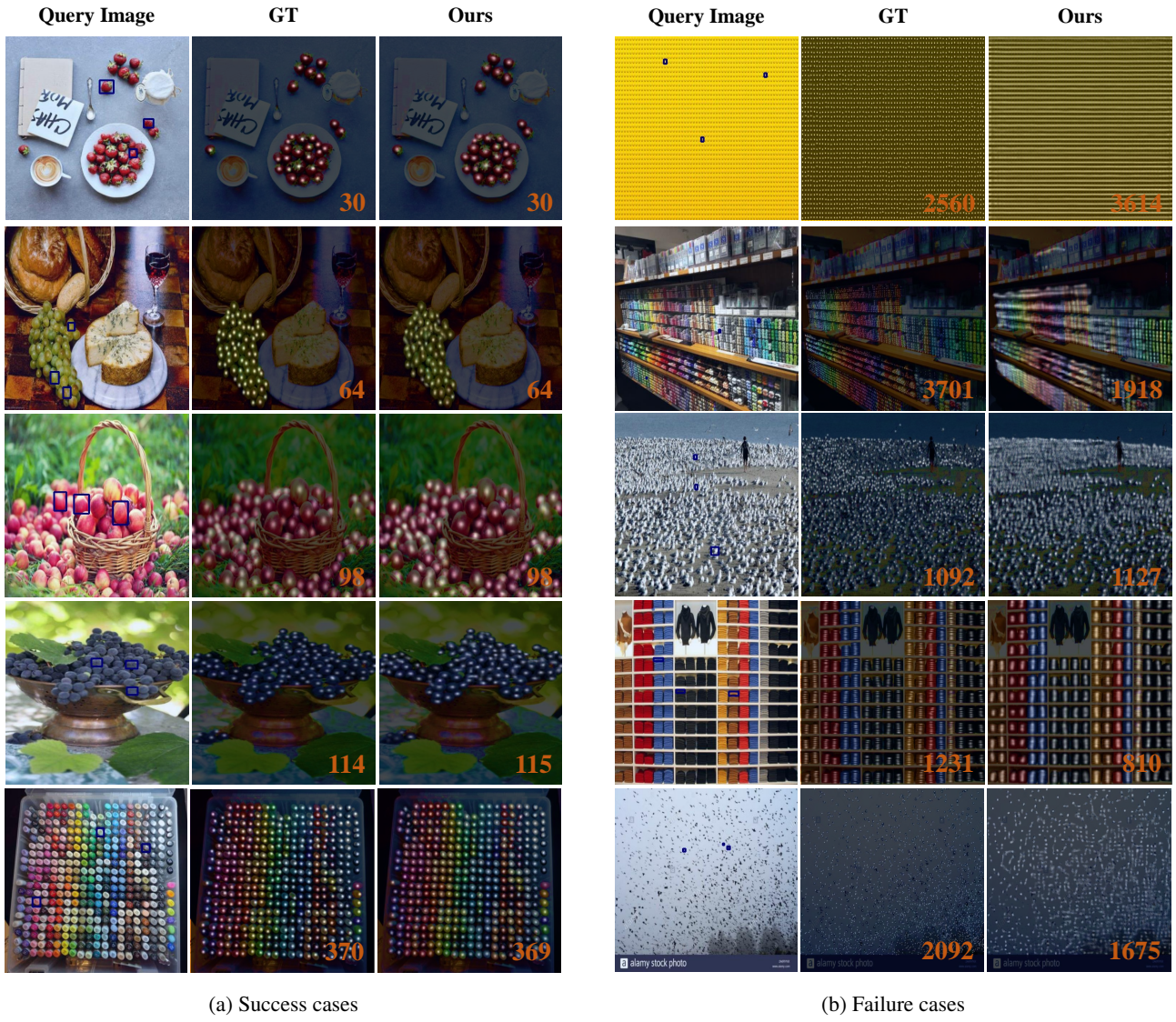


Figure 6: Additional Qualitative Results on FSC-147 dataset.

confusion problem through evaluations in a complex multi-class scenario, such as FSCD-LVIS and FSC-147-Multi. Moreover, we validate its effectiveness even in a single-class scenario. Experimental results validate the unique merits of our proposed method by achieving state-of-the-art performances and demonstrating its effectiveness in addressing the target confusion problem.

References

Arteta, C., Lempitsky, V., Zisserman, A., 2016. Counting in the wild, in: Computer Vision–ECCV 2016: 14th European Conference, Amsterdam, The Netherlands, October 11–14, 2016, Proceedings, Part VII 14, Springer, pp. 483–498.

Carion, N., Massa, F., Synnaeve, G., Usunier, N., Kirillov, A., Zagoruyko, S., 2020. End-to-end object detection with transformers, in: Computer Vision–ECCV 2020: 16th European Conference, Glasgow, UK, August 23–28, 2020, Proceedings, Part I 16, Springer, pp. 213–229.

Caron, M., Touvron, H., Misra, I., Jégou, H., Mairal, J., Bojanowski, P., Joulin, A., 2021. Emerging properties in self-supervised vision transformers, in: Proceedings of the IEEE/CVF International Conference on Computer Vision, pp. 9650–9660.

Djukić, N., Lukežić, A., Zavrtanik, V., Kristan, M., 2023. A low-shot object counting network with iterative prototype adaptation, in: Proceedings of the IEEE/CVF International Conference on Computer Vision, pp. 18872–18881.

Dosovitskiy, A., Beyer, L., Kolesnikov, A., Weissenborn, D., Zhai, X., Unterthiner, T., Dehghani, M., Minderer, M., Heigold, G., Gelly, S., Uszkoreit, J., Houlsby, N., 2021. An image is worth 16x16 words: Transformers for image recognition at scale. *ICLR*.

Gao, B.B., Huang, Z., 2024. Cstrans: Correlation-guided self-activation transformer for counting everything. *Pattern Recognition* , 110556.

Gong, S., Zhang, S., Yang, J., Dai, D., Schiele, B., 2022. Class-agnostic object counting robust to intraclass diversity, in: European Conference on Computer Vision, Springer, pp. 388–403.

He, K., Chen, X., Xie, S., Li, Y., Dollár, P., Girshick, R., 2022. Masked autoencoders are scalable vision learners, in: Proceedings of the IEEE/CVF conference on computer vision and pattern recognition, pp. 16000–16009.

Hsieh, M.R., Lin, Y.L., Hsu, W.H., 2017. Drone-based object counting by spatially regularized regional proposal network, in: Proceedings of the IEEE international conference on computer vision, pp. 4145–4153.

Leibe, B., Seemann, E., Schiele, B., 2005. Pedestrian detection in crowded scenes, in: 2005 IEEE computer society conference on computer vision and pattern recognition (CVPR'05), IEEE, pp. 878–885.

Liang, D., Chen, X., Xu, W., Zhou, Y., Bai, X., 2022. Transcrowd: weakly-supervised crowd counting with transformers. *Science China Information Sciences* 65, 160104.

Lin, W., Yang, K., Ma, X., Gao, J., Liu, L., Liu, S., Hou, J., Yi, S., Chan, A.B., 2022. Scale-prior deformable convolution for exemplar-guided class-agnostic counting, in: 33rd British Machine Vision Conference 2022, BMVC 2022, London, UK, November 21-24, 2022, BMVA Press, p. 313. URL: <https://bmvc2022.mpi-inf.mpg.de/313/>.

Liu, C., Zhong, Y., Zisserman, A., Xie, W., 2022. Countr: Transformer-based generalised visual counting, in: 33rd British Machine Vision Conference 2022, BMVC 2022, London, UK, November 21-24, 2022, BMVA Press, p. 370. URL: <https://bmvc2022.mpi-inf.mpg.de/370/>.

Lu, E., Xie, W., Zisserman, A., 2019. Class-agnostic counting, in: Computer Vision–ACCV 2018: 14th Asian Conference on Computer Vision, Perth, Australia, December 2–6, 2018, Revised Selected Papers, Part III 14, Springer, pp. 669–684.

Meng, D., Chen, X., Fan, Z., Zeng, G., Li, H., Yuan, Y., Sun, L., Wang, J., 2021. Conditional detr for fast training convergence, in: Proceedings of the IEEE/CVF International Conference on Computer Vision, pp. 3651–3660.

Nguyen, T., Pham, C., Nguyen, K., Hoai, M., 2022. Few-shot object counting and detection, in: European Conference on Computer Vision, Springer, pp. 348–365.

Ramachandran, P., Parmar, N., Vaswani, A., Bello, I., Levskaya, A., Shlens, J., 2019. Stand-alone self-attention in vision models. *Advances in neural information processing systems* 32.

Ranjan, V., Sharma, U., Nguyen, T., Hoai, M., 2021. Learning to count everything, in: Proceedings of the IEEE/CVF Conference on Computer Vision and Pattern Recognition, pp. 3394–3403.

Shi, M., Lu, H., Feng, C., Liu, C., Cao, Z., 2022. Represent, compare, and learn: A similarity-aware framework for class-agnostic counting, in: Proceedings of the IEEE/CVF Conference on Computer Vision and Pattern Recognition, pp. 9529–9538.

Stewart, R., Andriluka, M., Ng, A.Y., 2016. End-to-end people detection in crowded scenes, in: Proceedings of the IEEE conference on computer vision and pattern recognition, pp. 2325–2333.

Tran, N.H., Huy, T.D., Duong, S.T., Nguyen, P., Hung, D.H., Nguyen, C.D.T., Bui, T., Truong, S.Q., VinBrain, J., 2022. Improving local features with relevant spatial information by vision transformer for crowd counting, in: British Machine Vision Conference.

Wang, M., Cai, H., Han, X.F., Zhou, J., Gong, M., 2022. Stnet: Scale tree network with multi-level auxiliator for crowd counting. *IEEE Transactions on Multimedia* 25, 2074–2084.

Wang, M., Cai, H., Zhou, J., Gong, M., 2021. Interlayer and intralayer scale aggregation for scale-invariant crowd counting. *Neurocomputing* 441, 128–137.

Wang, M., Wang, X., 2011. Automatic adaptation of a generic pedestrian detector to a specific traffic scene, in: The 24th IEEE Conference on Computer Vision and Pattern Recognition, CVPR 2011, Colorado Springs, CO, USA, 20–25 June 2011, IEEE Computer Society, pp. 3401–3408. URL: <https://doi.org/10.1109/CVPR.2011.5995698>, doi:10.1109/CVPR.2011.5995698.

Yan, Z., Yuan, Y., Zuo, W., Tan, X., Wang, Y., Wen, S., Ding, E., 2019. Perspective-guided convolution networks for crowd counting, in: Proceedings of the IEEE/CVF international conference on computer vision, pp. 952–961.

Yang, S.D., Su, H.T., Hsu, W.H., Chen, W.C., 2021. Class-agnostic few-shot object counting, in: Proceedings of the IEEE/CVF Winter Conference on Applications of Computer Vision, pp. 870–878.

Yin, Z., Wang, P., Wang, F., Xu, X., Zhang, H., Li, H., Jin, R., 2022. Transfgu: a top-down approach to fine-grained unsupervised semantic segmentation, in: European Conference on Computer Vision, Springer, pp. 73–89.

You, Z., Yang, K., Luo, W., Lu, X., Cui, L., Le, X., 2023. Few-shot object counting with similarity-aware feature enhancement, in: Proceedings of the IEEE/CVF Winter Conference on Applications of Computer Vision, pp. 6315–6324.

Zhang, Y., Zhou, D., Chen, S., Gao, S., Ma, Y., 2016. Single-image crowd counting via multi-column convolutional neural network, in: Proceedings of the IEEE conference on computer vision and pattern recognition, pp. 589–597.